ACS APPLIED ENERGY MATERIALS

www.acsaem.org Article

Comparing the Solid Electrolyte Interphases on Graphite Electrodes in K and Li Half Cells

Franziska Allgayer, Julia Maibach, and Fabian Jeschull*

Cite This: https://doi.org/10.1021/acsaem.1c03491 Read Online

ACCESS | Metrics & More | Article Recommendations | Supporting Information

ABSTRACT: In both Li-ion and K-ion batteries, graphite can be used as the negative electrode material. When potassium ions are stored electrochemically in the graphite host, the electrode capacities fade faster than in the lithium ion counterpart. This could be due to the high reactivity of the potassium metal counter electrode (CE) in half cells or a less stable solid electrolyte interphase (SEI) in the potassium case. Previous surface studies on graphite electrodes cycled in K half cells have focused on the SEI characteristics of different electrolyte formulations or different states of charge. In this study, we exploit the fact that graphite can store both lithium and potassium ions. Cell and component parameters have been largely maintained the same, with the only differences between Li and K half cells being the cation of the electrolyte salt and the alkali metal at the CE. The SEI layers formed under these conditions in either setup are studied using X-ray photoelectron spectroscopy with the aim to draw a direct comparison between the surface layers in both charged and discharged states. The results show a considerable crosstalk under OCV conditions between K-metal and the working electrode. Furthermore, the relative SEI layer composition after cycling varies considerably between Li and K half cells. Different dominant SEI species are present depending on the alkali metal used. The strong capacity fade observed in graphite−K half cells is likely linked to much smaller concentrations of inorganic compounds, such as KF, and increased amounts of organic compounds in the SEI.

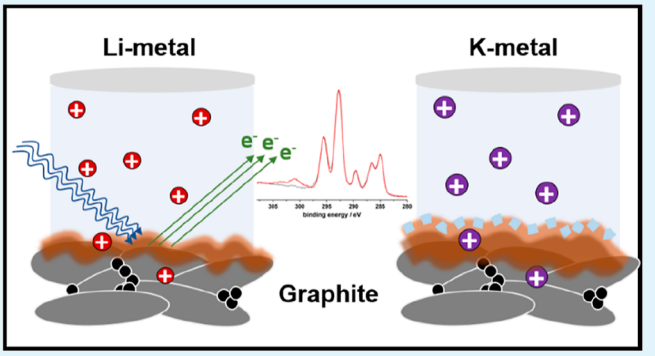

KEYWORDS: *XPS, X-ray photoelectron spectroscopy, potassium-ion battery, KIB, lithium-ion battery, LIB, graphite, solid electrolyte interphase, SEI*

INTRODUCTION

With the exception of sodium ions, graphite is able to form binary intercalation compounds with alkali metal ions in a reversible electrochemical reaction. In the case of Li-ions, the specific capacity is 372 mA h g^{-1} (LiC_6), whereas the intercalation of K-ions yields a lower specific capacity of 279 mA h g^{-1} (KC_8) as a result of their higher atomic weight and the different stoichiometry of the intercalation compound.[1] Nonetheless, graphite electrodes are an attractive choice as anodes for K-ion batteries (KIBs) owing to their comparatively low average operation potential (E_{avg} = 200 mV vs K/K^+) and their plateau-like potential profile.[2] The recent results demonstrate that the first-cycle Coulombic efficiencies (CEs) are considerably lower, and capacity fading proceeds much faster in graphite−K half-cell setups than in the corresponding Li system.[3,4] This is partly related to the fact that graphite expands by 60% upon intercalation of K-ions, but only up to 10% upon intercalation of Li-ions,[5] thus exposing the active material particles to more stress and strain and, as a consequence, rapid material fatigue. A recent study further suggests that potassium intercalation is far more sensitive to graphite properties, such as the interlayer distance, crystallinity, and stacking faults, than the lithium intercalation process, leading to significant differences in the resulting specific capacity and capacity retention.[6]

In addition, the solid electrolyte interphase (SEI) that is formed from surface deposits as a result of electrolyte degradation reactions plays a vital role in passivating the electrode surface and in preventing recurrent degradation processes at the electrode−electrolyte interface. The SEI is a heterogeneous surface layer comprising of various organic and inorganic compounds that is permeable to the cations but prevents cointercalation of solvent molecules that could lead to graphite exfoliation.[7] Typically, inorganic compounds are found closer to the electrode surface, while more organic species are found in the outer regions.[8] The strong expansion of the active material can readily cause fractures in the SEI

Received: November 7, 2021
Accepted: December 10, 2021

layer that leads to recurrent SEI formation reactions as the extensive research on Si electrodes has shown.[9] Therefore, as more and more electrolyte components are consumed, the SEI layer grows continuously with increasing cycle number, thus leading to consumption of the K-inventory in the process.

A first step in understanding the complex surface chemistry of cycled battery electrodes is to characterize SEI components using surface-sensitive analytical techniques, such as X-ray photoelectron spectroscopy (XPS). Naylor et al.[10] recently employed a photoelectron spectroscopy depth profiling approach using different excitation energies at a synchrotron source, showing that already on the first cycle a comparatively thick SEI layer is formed on graphite cycled in a K-ion half cell. The authors further observed considerable changes in the SEI layer thickness and composition that are induced presumably due to the graphite volume expansion and contraction upon intercalation and deintercalation of K-ions. Moreover, Madec et al.[11] observed a significant degree of "crosstalk" in half-cell setups that employ the K-metal as a counter electrode (CE). The reaction at the potassium electrode leads to the formation of decomposition products that diffuse to the graphite electrode and deposit on the electrode surface, thus affecting the overall SEI composition. It is worth mentioning that previous studies on the SEI stability in sodium-ion batteries arrived at similar conclusions and attributed this issue to the formation of soluble degradation products that adversely affect the cell performance and the formation of a less-protective SEI layer.[12−14]

Because both potassium and lithium ions intercalate into graphite, there is an opportunity for a direct comparison between the SEI layers formed on cycled graphite electrodes in either Li or K half-cell configurations. In this study, we exploited this fact and prepared XPS samples under the same conditions, using the same cell components (with exception of the alkali metal ions and the CE) and the same cell parameters. The results presented herein provide a detailed picture of the graphite interfaces in the Li and K half-cell setups under open circuit conditions and after SEI formation in the charged and discharged state, respectively. Furthermore, our results indicate how irreversible reactions at the graphite electrode interface in KIBs could be mitigated in the future using SEI design approaches.

EXPERIMENTAL DETAILS

Materials. Graphite powder (SFG 6L) and carbon black (Super C65) were obtained from Imerys Graphite & Carbon, and CMC−Na was acquired from Merck. Electrolyte solvents, ethylene carbonate (EC, >99%, anhydrous, BASF), and diethyl carbonate (DEC, Merck, >99%) were used as received. Whatman GF/B separators were dried before use at 120 °C for 12 h under vacuum. Celgard 2325 separators were stored in the glovebox antechamber under vacuum overnight before use. K_3PO_4 (Merck, reagent grade, >98%), KF (Merck, ACS reagent >99.0%), K_2CO_3 (Merck, anhydrous, 99.0%), CH_3COOK (Merck, ACS reagent, >99.0%), and NaCl (Merck, ACS reagent, >99.0%) were used as received. The electrolyte salts $LiPF_6$ (Merck, battery grade) and KPF_6 (Merck, >99%) were dried at 120 °C for 12 h under vacuum. Lithium discs (PI-KEM, purity: 99.9%, 250 μm thick, 16 mm in diameter) were used as received. Potassium ingots (99.95%) were purchased from Merck.

Electrode Preparation, Cell Assembly, and Testing. *Electrode Preparation.* Graphite electrodes consisted of a mixture of SFG 6L graphite, Super C65, and the CMC−Na binder in a weight ratio 95:1:4. First, 10 mL of a 2 wt % CMC−Na binder solution was prepared from 10 mL deionized water. Then, for the slurry preparation, 20 mg of Super C65 was added to 4 mL of the binder solution (80 mg CMC−Na) and the suspension was mixed for 5 min at 2000 rpm in a planetary mixer (Thinky, ARV-310P). A total of 1.9 g SFG 6L was added in two batches to the slurry and blended using the planetary mixer (5 min, 2000 rpm). The viscosity was controlled by adding deionized water between the mixing steps. The thus prepared electrode slurry was coated on copper foil with a doctor blade. The electrode coating was allowed to dry overnight under ambient conditions. Then, electrode discs were cut in a diameter of 14 mm, dried under vacuum at 120 °C for 12 h, and introduced into an Ar-filled glovebox without further exposure to air.

Cell Assembly. Half cells were built in a coin cell-type format (EL-cell, Germany) with a lithium or potassium counter−reference electrode. In the case of potassium CE, the metal was spread with a ceramic knife and spatula onto the back contact of the cell. The lithium CE was a circular disc with a 16 mm diameter and a 250 μm thickness (Alfa Aesar). The graphite electrode (working electrode, WE) was covered by a layer of Celgard separator and a layer of Whatman separator. The separators were soaked in 150 μL electrolyte, that is, in 0.75 M $LiPF_6$ and KPF_6 dissolved in a mixture of EC and DEC (v/v = 1:1), respectively.

Cell Testing. The half cells were cycled for 1.5 ("charged") and 2 cycles ("discharged") either on a VMP-300 or a BCS battery cycler (both Biologic, France). The cells were tested using a constant current (CC)−constant potential (CP) cycling protocol at a rate of C/20 [1 C = 372 mA h g^{-1} (Li) and 279 mA h g^{-1} (K)] between the potential limits of 0.01 and 1.20 V versus Li/Li^+ and K/K^+, respectively. The cutoff condition during the CP-step was a limiting current of C/40 (half the current of the CC-step). Besides, after each galvanostatic sequence, a potentiostatic sequence was added (CC−CP-protocol).

X-ray Photoelectron Spectroscopy. Reference samples and pristine electrodes were generally handled under ambient conditions. The measurements were carried out on a Thermo Scientific K-alpha+ X-ray photoelectron spectrometer. Battery samples (OCV and cycled samples) were strictly handled under inert gas conditions in a glovebox and transferred between the glovebox and spectrometer without exposure to air or moisture. The measurements were conducted on a Thermo Scientific K-alpha XP-spectrometer equipped with a glovebox compartment for inert gas transfers. In both spectrometers, a monochromized Al Kα X-ray source was used with an excitation energy of 1486.6 eV. On each sample surface, a full set of spectra was acquired from at least two different spots. Data analysis was performed with Avantage (software version 5.9904, Thermo Scientific). For background subtraction, the "smart background" function was used (Shirley background with an additional constraint that the background function is not greater than any datapoint in the measured region). For peak fitting, Voigt profiles were used with a Lorentzian contribution of 20−30%. Graphite signals were fitted with an asymmetric tail. The spectra were referenced to the saturated hydrocarbon, that is, the sp^3-C−C/CH peak in the C 1s spectra. The fitted data were then exported to Origin (2018b) for plotting.

Reference Measurements. Powder samples for reference measurements were ground using a mortar. Four different measurement conditions were studied: the neat powder applied on double-sided conductive copper tape and either mounted on the sample holder directly (grounded conditions) or placed on a piece of scotch tape (floating conditions) to prevent electronic contact with the sample holder. Another fraction of the powder was blended with ground NaCl as internal binding energy (BE) reference and then measured under grounded and floating conditions. For referencing, the CH signal of the glue of the sticky Cu tape was used.

Battery Electrodes. Pristine electrodes were mounted on the sample holder without further preparation steps. OCV and cycled XPS samples were extracted from the cells and then rinsed with DMC before mounting on the sample holder (grounded conditions; the current collector foil was in contact with the sample holder). The samples were transferred under inert gas conditions, as stated above. Unless stated differently, measurements were conducted without charge neutralization. In cases where a neutralizer was used, the spectra were recorded as iteration scans. This way, individual spectra

https://doi.org/10.1021/acsaem.1c03491
ACS Appl. Energy Mater. XXXX, XXX, XXX−XXX

Table 1. Reference Measurements on Various Potassium Salts with NaCl as the Internal Standard

	reference signals			sample binding energies/eV (atomic concentration/atom %)					
sample	C 1s	Na 1s	Cl 2p	K $2p_{3/2}$	C 1s	O 1s	P $2p_{3/2}$	F 1s	atomic ratios
K_2CO_3[b]	285	1071.1	198.5	292.9 *(13.3)*	289.1 *(10.8)*	531.0 *(36.62)*			K/C/O *1.00:0.81:2.75*
CH_3COOK[a]	285	1071.3	198.3	292.7 *(13.37)*	*C1:* 285.0 *(32.99)*	531.2 *(28.67)*			K/C1/C2/O *1.00:2.47:1.08:2.15*
					C2: 288.3 *(14.46)*				
KPF_6[a]	285	1071.9	198.9	294.8 (6.4)			137.8 (7.03)	687.9 (45.6)	K/P/F *1.00:1.06:6.82*
Impurity (KF, KPF_x Cl_y?)			*195.1* (2.94)	*293.7* (2.59)				*683.4* (0.94)	
KF[a]	285			292.7 (42.08)				683.4 (38.15)	K/F *1.00:0.91*
K_3PO_4[b]	285	1071.2	198.6	292.9 (18.13)		530.4 (20.79)	132.3 (5.18)		K/P/O *1.00:0.29:1.14*
Cu-tape	285			C1:285/C2:286.5/C3:288.9		O1: 532.1, O2: 533.6			

[a]Floating conditions. [b]Grounded conditions.

were received after each scan in order to exclude damage to the sample surface from the charge compensation system over extended acquisition times. The spectra were later collapsed into one spectrum in the Avantage software.

RESULTS AND DISCUSSION

Reference Measurements on Potassium Salts. When reference to common XPS databases, such as the NIST XPS database,[15] only a few literature entries appear for characteristic potassium salts that are expected as SEI components. Therefore, in this first part a small XPS reference table was generated to confirm binding energies from relevant and existing entries (KF, K_3PO_4, and CH_3COOK), as well as to add new entries of SEI-characteristic compounds such as K_2CO_3 and KPF_6. In addition, our results are compared to a recently published work of Caracciolo et al.[16] for validation.

The reference measurements were carried out on powder samples stuck on double-sided copper tape. The samples were studied under grounded and "floating potential" conditions. In the latter case, the conductive tape was placed on a layer of scotch tape that prevented direct electronic contact between the sample and sample holder. The idea of this approach was to avoid conditions in which some particles are in good electronic contact while others are not, which would result in different BE shifts of the same components due to charging effects. Ideally, all particles would then experience the same surface potential and thus the same BE shifts. However, this was not the case for all samples and in addition peak broadening was observed. For the reference values presented in Table 1, the most reliable set of XPS data was chosen out of the two measurement conditions based on peak shapes, BE positions with respect to an internal standard, and the relative atomic ratio compared to the expected stoichiometric composition (indicated in table). The corresponding XPS spectra are provided in the Supporting Information (Figures S1−S5). As the internal reference, NaCl was added to each sample (except KF, which showed some changes in the XPS spectra when blended with NaCl). The spectra were referenced to the CH/sp^3-C signal of the glue of the Cu-tape at 285 eV. Comparing the positions of the Na 1s and Cl $2p_{3/2}$ signals of NaCl across different samples (with exception of the KPF_6 sample) results in average binding energies of 1071.2 ± 0.1 eV (Na 1s) and 198.46 ± 0.16 eV (Cl $2p_{3/2}$), respectively. An additional signal is observed from the Na KLL Auger line at around 536 eV in the O 1s spectra. As will be outlined further below, the KF and KPF_6 samples behaved somewhat different from the rest of the set.

Generally, the BE difference between the Na 1s and Cl $2p_{3/2}$ signals should be the same for all samples, independent of variations in the absolute BE shift and is within a small margin of less than ±0.1 eV (which is the energy step size data acquisition) for samples measured under the same conditions, that is, the BE difference measured under floating potential conditions is 873 and 872.6 eV under grounded conditions. The BE range of the C 1s-measurements was enlarged because the K 2p signals appear just above the C 1s region between 290 and 300 eV. Based on the spin−orbit splitting, the characteristic BE difference between the K $2p_{3/2}$ peak and the K $2p_{1/2}$ peak is 2.8 eV (intensity ratio 2:1). Comparing the K $2p_{3/2}$ BE positions, it can be further seen that all potassium salts, except KPF_6, are observed in the narrow range between 292.7 and 292.9 eV with respect to the CH/sp^3-C signal at 285 eV.

The C 1s signal of $LiCO_3$ is commonly reported in the BE range between 289.5 and 290 eV.[7] Other alkali or alkaline earth carbonates are found in the NIST database[15] in the same BE region. The observed 289.1 eV for K_2CO_3 is at the lower end of the reported BE shifts for carbonate salts. Previously reported BEs for K_2CO_3 lie in the range of 288.6−289.0 eV.[16,17] Differences may also relate to slightly different points of reference. For potassium acetate (CH_3COOK), the signal intensity of the CH_3-group is overlapping with the signal of the Cu-tape at 285 eV, which leads to a significant overestimation of the atomic ratio for this carbon signal. The carboxylate signal (−(C═O)OK) is located at 288.3 eV at slightly lower BE than the CO_3^{2-} component in K_2CO_3. The atomic ratios for potassium, oxygen, and carbon within the carboxylate unit agree well with the expected stoichiometric ratio of 1:1:1:2 (K/C1/C2/O). In the corresponding O 1s spectra, the −(C═O)O− (CH_3COOK) and CO_3^{2-} (K_2CO_3) signals show up at 531.2 and at 531.0 eV, respectively. In the following SEI analysis, the two components were thus fitted as one signal, as they cannot be easily separated given such a high spectral overlap.

https://doi.org/10.1021/acsaem.1c03491
ACS Appl. Energy Mater. XXXX, XXX, XXX−XXX

The K $2p_{3/2}$ signal of KPF_6 exhibits a notable shift toward higher binding energies (294.8 eV), which is about 1.9−2.1 eV higher than the K-signal of the other salts examined herein. In addition, the salt shows an additional K 2p doublet from another impurity compound in a significant concentration. The data suggest that several impurities are present. For example, in the F 1s spectrum, a signal at 683.4 eV is observed, which coincides with the F 1s signal of fluoride in the KF sample. The BE of this component is also in agreement with previous studies.[10] However, the elemental distribution suggests that KF cannot account for the entire amount of impurities in the sample (the K 2p signal is about 2.5 times as intense as the F 1s component in terms of the atomic concentration). Instead, a second chlorine containing component also appears to be present. The presence of chlorine impurities, indicated by an additional signal in the Cl 2p spectrum (Figure S3), is not entirely surprising, given that many PF_6^- salts are synthesized from phosphorous chlorides. However, the amount of the impurity is quite significant and may cause corrosion problems at high potentials.[18] Reactions of PF_6^- with NaCl in the sample were excluded on the basis of the expected 1:1 atomic ratio between the Na 1s (10.5 atom %) and Cl $2p_{3/2}$ (9.6 atom %) signals. Another possibility is radiation damage under degradation of a fraction of the salt. The P 2p spectrum shows one doublet at 137.7 eV ascribed to PF_6^-, which is the same BE region as the corresponding Li-salt.[8] The phosphorous signal of the phosphate anion in K_3PO_4 is seen at a considerably lower BE of 132.3 eV (P $2p_{3/2}$). Any decomposition products in the SEI layer that relate to the formation of alkali fluorophosphates ($(OR)_x(P{=}O)F_y$) are expected in the BE region between the signals of PO_4^{3-} and PF_6^-. Overall, the expected atomic ratio of K/P/O of 3:1:4 is in good agreement with the experimentally found ratio of 3.5:1:4, despite a slight overestimation of the K concentration.

Electrode Crosstalk in Half-Cell Configurations. In a first step to characterize the electrode surface of graphite electrodes in both Li and K half-cell configurations, we have investigated graphite electrodes stored in the electrolyte against either a Li/K CE (in the following referred to as "OCV samples") or a stainless steel coin cell spacer, that is, CE free (in the following referred to as "CE-free samples").

The complete set of the spectra for the pristine, CE-free, and the OCV samples is provided in Figures S6−S11. Shown in Figure 1 are the C 1s spectra of the pristine and the two CE-free samples that were stored either in the Li- or K-containing electrolyte formulation. The samples were rinsed with DMC after extraction from the coin cell and do not show any indication of solvent residues or surface-adsorbed species that could be attributed to carbon-containing compounds in the electrolyte. In fact, the spectra nearly coincide when normalized to the maximum intensity. The CE-free sample stored in the K-electrolyte shows a K 2p doublet signal above 290 eV, which is attributed to an ion exchange between sodium and potassium ions at the carboxymethyl groups of the CMC−Na binder due to the vast excess of potassium ions in solution. In accordance with this finding, no Na 1s signal was observed for this sample. In contrast, in the case of the CE-free sample stored in the Li-electrolyte, a Na 1s signal could still be detected on the graphite surface.

The effect of the selected alkali metal as CE (OCV samples) on the surface composition of the graphite electrode is shown in the C 1s−K 2p spectra in Figure 2. The spectra have been referenced to the sat. hydrocarbon peak at 285 eV. The XPS

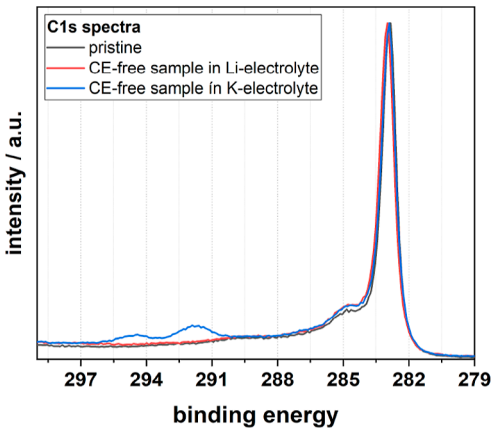

Figure 1. Comparison of the C 1s spectra of a pristine graphite electrode and two graphite electrodes stored either in a $LiPF_6$ or a KPF_6 electrolyte against a coin cell spacer. The spectra were normalized to the maximum peak height for this comparison.

spectrum of the pristine sample comprises of a prominent graphite (C−C, sp^2) signal (gray color) and minor contributions from oxidized carbon species originating from surface groups, such as epoxides or carboxylic acids. As demonstrated in Figure 2b, even after 4 days in the Li-electrolyte (750 mM $LiPF_6$, EC/DEC v/v = 1:1), the CE-free sample shows little to no change from the C 1s spectrum of the pristine electrode in the C 1s region. When a Li CE is added to this setup and stored for a similar time interval (Figure 2c), the graphite peak exhibits a shoulder toward higher BEs. This shoulder can be fitted with an additional peak allowing the fitting parameters for asymmetric peak shape for the graphite peak to be kept constant. The shoulder indicates the superposition of the graphite and the sat. hydrocarbon peak signal. The distance between these two peaks became smaller in this sample, that is, when stored against a Li−metal CE. The neighboring peak, indicated in blue and centered at 287.0 eV, was assigned to CO species. Furthermore, carbonyl (C═O) and carbonate species (CO_3), although minor components, are clearly visible in the spectrum. These changes suggest the presence of surface deposits on the surface of the OCV samples induced by the Li−metal CE.

However, the chemical changes to the graphite surface when stored in a Li-electrolyte against Li−metal are negligibly small when compared to the considerable differences between the CE-free (Figure 2e) and OCV sample (Figure 2f) of the corresponding K half-cell configurations: from the intensity of the K 2p signal relative to the graphite signal it can be seen readily that in the presence of a K-metal CE, the amount of K-salt deposits is evidently higher. Similarly, the $-CH_2-$ and −CO− signals have notably increased when replacing the stainless steel spacer by potassium. Intensity changes in the higher BE range have also occurred, as can be clearly seen from the peak in the CO_3 region.

These results strongly suggest a migration process of decomposition products from the CE to the WE, which is also commonly referred to as the "crosstalk" phenomenon.[11] The results are in accordance with a study by Madec et al.,[11] previously reporting similar surface changes on Sb electrodes (comprising Sb, carbon black, and vapor grown carbon fibers) in K half cells. Our comparison with a Li half cell highlights that the reactivity of the K-metal CE cannot be ignored in XPS measurements on electrodes aged in half-cell configurations, as

https://doi.org/10.1021/acsaem.1c03491
ACS Appl. Energy Mater. XXXX, XXX, XXX−XXX

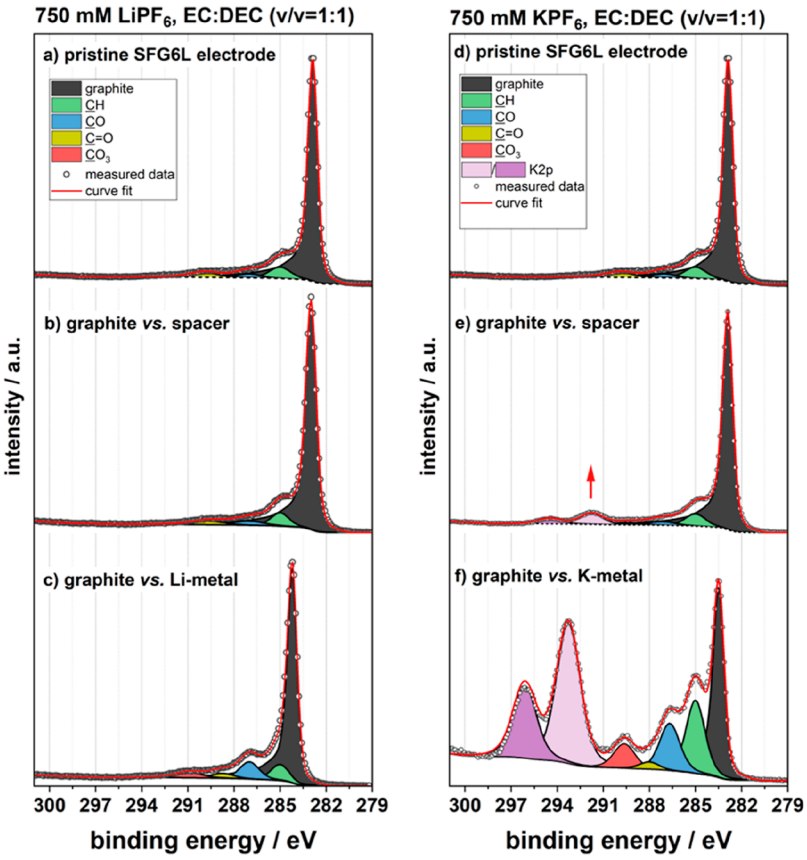

Figure 2. C 1s−K 2p spectra of Li−graphite [left panel; (a−c)] and K−graphite [right panel; (d−f)] half cells. (a, d) Pristine graphite electrode, (b, e) graphite stored in the electrolyte against the coin cell spacer (CE-free), and (c, f) graphite stored in the electrolyte against the Li- or K-metal.

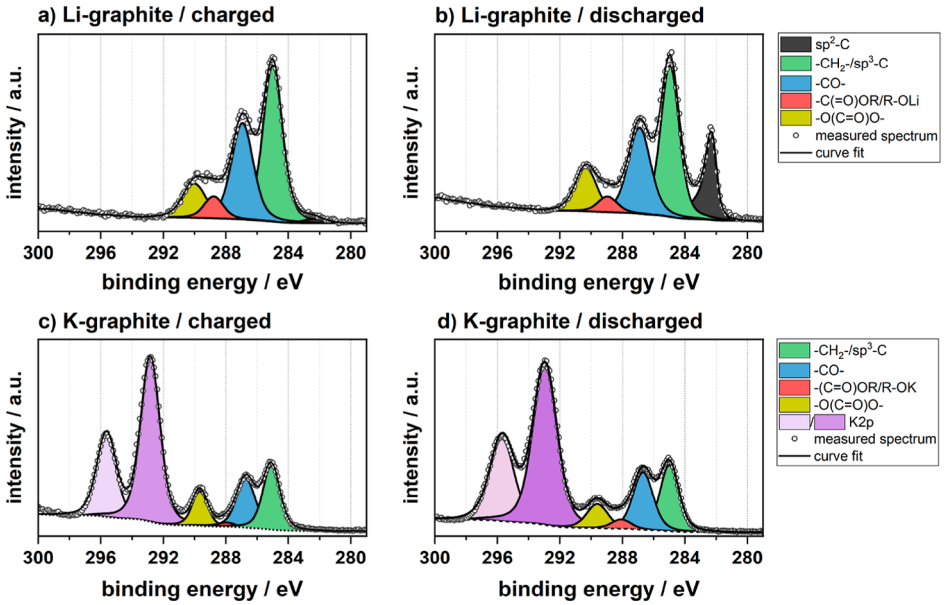

Figure 3. C 1s−K 2p-spectra of the graphite electrode surface after charge, that is, in the intercalation stage (a, c) and after the discharge, that is, in the deintercalated stage (b, d).

the influence of crosstalk on the surface composition is significant, even after short storage times (i.e. 4 days) under OCV conditions.

SEI Composition in Charged and Discharged Graphite Electrodes. Cell cycling was conducted at a slow C-rate of C/25 for 1.5 (charged) and 2 cycles (discharged), respectively. The XPS analyses were thus performed in the fully charged (intercalated) and fully discharged (deintercalated) states. The corresponding voltage profiles are given in Figures S12 and S13 in the Supporting Information. The discharge capacity of Li−graphite cells was around 355 mA h g^{-1} and those of K−graphite cells around 265 mA h g^{-1}, which lie in the expected

https://doi.org/10.1021/acsaem.1c03491
ACS Appl. Energy Mater. XXXX, XXX, XXX−XXX

Table 2. Peak Positions and Normalized Peak Areas in the C 1s−K 2p BE Region of Cycled Li− and K−Graphite Electrodes in Either the Charged or Discharged State

	binding energies/eV (peak areas[a]/a.u.)						
sample	sp^2-C/graphite	$-CH_2-$/sp3-C	−CO−	−(C═O)OR/R−OX (X = Li, K)	−O(C═O)O−	K $2p_{3/2}$	K $2p_{1/2}$
Li−graphite/charged	282.4 (0.03)	285 (1.00)	286.9 (0.69)	288.8 (0.14)	290.0 (0.25)		
K−graphite/charged		285 (1.00)	286.6 (0.84)	287.9 (0.06)	289.6 (0.48)	292.8 (2.91)	295.6 (1.46)
Li−graphite/discharged	282.3 (0.46)	285 (1.00)	287.0 (0.68)	289.0 (0.11)	290.4 (0.33)		
K−graphite/discharged		285 (1.00)	286.7 (0.93)	288.1 (0.15)	289.6 (0.41)	293.0 (3.15)	295.7 (1.62)

[a]Peak areas normalized to the total peak area in the shown C 1s−K 2p binding region.

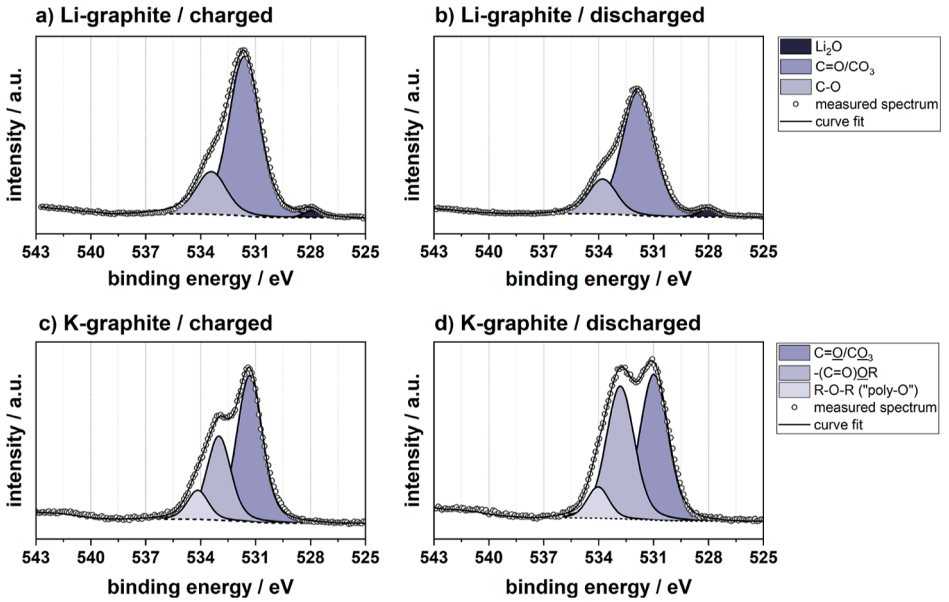

Figure 4. O 1s spectra of the graphite electrode surface after charge, that is, in the intercalation stage (a, c) and after the discharge, that is, in the deintercalation stage (b, d).

range in both cases. As previously reported,[3,5] the C.E. of the K−graphite cell is low in the first cycles, that is, 57.6% (cycle 1) and 83.2% (cycle 2). In comparison, the C.E. values of the corresponding Li−graphite system are 86.7% in the first and 99.4% in the second cycle.

C 1s−K 2p Spectra. Figure 3 shows the C 1s−K 2p region of the four electrode samples and the corresponding BEs and normalized peak areas are given in Table 2. The graphite electrodes cycled against a lithium CE (Figure 3a) show a common distribution of decomposition products[7,19,20] at the graphite surface comprising of CO species at around 287 eV, carboxylate and alcoholate species (−(C═O)OR−/R−OLi) at around 289 eV, as well as carbonate components (−O(C═O)O−) at about 290.0 eV. The spectra were referenced to the sat. hydrocarbon peak at 285 eV. At lower BE, there is also a signal from sp^2 carbon (C−C, sp^2), ascribed to carbon black and graphite (282.3 eV). While this signal is nearly absent in the charged state, it is clearly visible in the discharged state. The intensity of this bulk signal is an indication of the SEI layer thickness,[21] suggesting that the surface layer on graphite is thicker in the charged state than in the discharged state. It is worth noting that the C 1s spectrum of the discharged sample agrees well with previous in-house XPS data[22] on a similar electrode compositions based on water-soluble binder mixtures.

For the samples cycled in the K−graphite half cell, a strong K 2p signal centered at 293 eV (K $2p_{3/2}$) is observed. The intensity of the K 2p peaks in relation to the $-CH_2-$/sp^3-C−C signal is significantly larger than in the previous OCV samples, where the peak maxima between these two peaks had similar intensities. In contrast to the samples prepared in the lithium half cell, the C 1s−K 2p spectra recorded for the samples from the potassium half cell (Figure 3c,d) do neither show a graphite peak in the charged nor the discharged state. This implies that the surface layer at this early stage is already considerably thicker than in the corresponding lithium system. In fact, in our previous study, we found a rapidly increasing voltage hysteresis in the voltage profiles of K−graphite half cells,[3] which most likely relates to overpotentials building up at the electrode−electrolyte interface during cycling. In a recent photoelectron spectroscopy depth profiling study by Naylor et al.,[10] the authors were also able to show a strong attenuation of the graphite signal after only one cycle. To probe through the entire SEI layer in the K-ion case, higher excitation energies are therefore necessary. It is evident from previous reports[10,23] and the current results that the SEI growth proceeds considerably faster in K-systems compared to Li-systems. The above-described crosstalk also contributes to this effect. A major contributor to increased degradation at the electrode interface is likely due to the larger volume expansion of up to 60% during potassium intercalation (as compared to about 10% for Li). The electrode thus experiences more stress and strain, which may lead to recurrent SEI formation/electrolyte decomposition in places where the SEI cracked.

https://doi.org/10.1021/acsaem.1c03491
ACS Appl. Energy Mater. XXXX, XXX, XXX−XXX

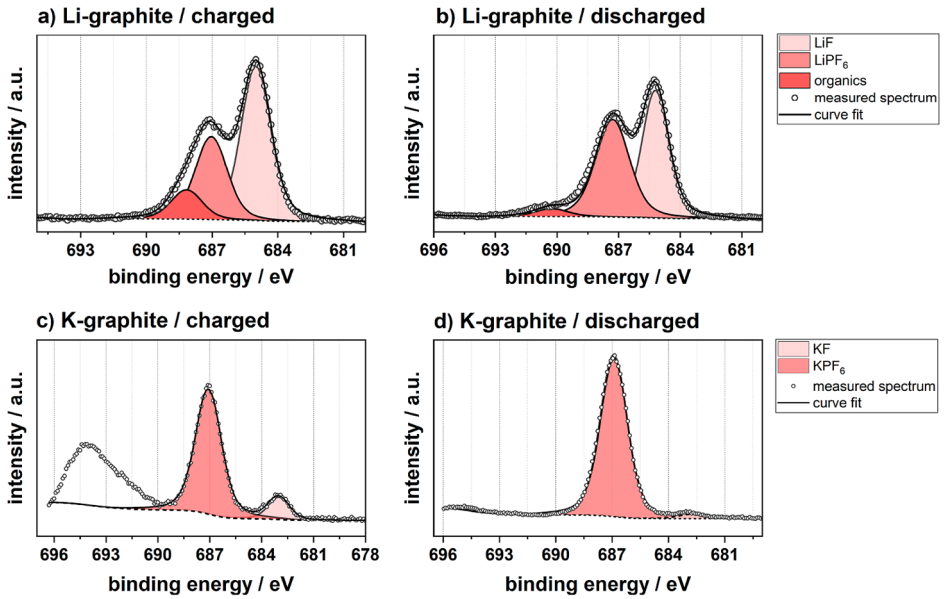

Figure 5. F 1s spectra of the graphite electrode surface after charge, that is, in the intercalation stage (a, c) and after the discharge, that is, in the deintercalation stage (b, d).

In the BE range above 285 eV, the CO component is located at 286.7 eV and the −(C═O)OR−/R−OK is observed at around 288 eV. Especially in the charged sample, the latter peak is a minor component and thus its position and peak area is associated with a larger uncertainty. The carbonate compounds are observed at 289.6 eV. The BEs of these two species are found in the same BE region as the reference salts CH_3COOK and K_2CO_3 presented above (Table 1). Overall, it can be stated that the peaks of C 1s components in higher oxidation states are generally located at slightly lower BEs than in the corresponding C 1s spectra of the Li−graphite samples (Table 2). As these peaks are a superposition of compounds with similar BEs, changes in their relative ratios can lead to a shift in the peak center.

The peak areas in Table 2 are normalized to the peak area of the CH-peak for a straightforward comparison of relative intensity differences between samples. The results show that the CO-component is more prominent on graphite electrodes cycled against potassium, compared to the lithium half cells. As mentioned above, the −(C═O)OR−/R−OK undergoes a considerable intensity change from the charged (nearly absent) to the discharged sample. The carbonate content in the graphite−K cells is also larger than in the corresponding graphite−Li half cells, which is a result of higher degrees of electrolyte decomposition and in accordance with a thicker SEI layer.

O 1s Spectra. The comparison of the O 1s environments of Li−graphite and K−graphite samples (Figure 4) shows some general differences in the SEI composition on these electrode surfaces. In the spectra of the Li−graphite samples, a minor component is observed at 528 eV that is ascribed to Li_2O. The most intense peak is seen at 531.6 eV for the electrode in the charged state (Figure 4a) and 531.8 eV for discharged sample (Figure 4b) and is assigned to carbonate and carboxylate components. The peaks at 533.4 eV (charged) and 533.7 eV (discharged) in the same spectra are assigned to CO species.

A potassium oxide component was not observed in the O 1s spectra of the K−graphite samples (Figure 4c,d). C═O/CO_3 is centered at 531.2 eV (charged) and 531.1 eV (discharged), which coincides well with the peak positions determined for the CH_3COOK and K_2CO_3 reference samples measured in the first part of this study (Table 1). The reference measurements showed that the O 1s signals of two compounds are spaced closely together in BE. Because the BE difference of both peaks is smaller than their full width at half-maximum (FWHM), signals from C═O and CO_3 species were fitted as a single peak with peaks widths (FWHM) of 1.64 (charged) and 1.81 (discharged), respectively. For comparison, the FWHM for the corresponding peaks in the spectra of the Li−graphite samples was larger with 2.0−2.1, which may indicate that oxygen in Li_2CO_3 and CH_3COOLi displays a larger BE difference. Also, the reference samples are merely representatives of possible compounds in the SEI layer and mainly act as an orientation to pinpoint species of similar chemical nature.

Moreover, the O 1s data show that the CO component is more prominent with respect to the C═O/CO_3 peak in the SEI layer of K−graphite samples. This finding is in general accordance with relative peak intensity ratios observed in the C 1s−K 2p spectra, where the peak area ratios between the CO and CH_2/sp^3-C peaks are larger than in the case of the corresponding Li−graphite samples. Also, in the O 1s spectra of the K−graphite samples, the CO peak position has shifted toward lower binding energies by 0.6−0.8 to 532.8 eV (charged) and 532.9 eV (discharged). An additional component was observed at 534.0 eV that was ascribed to oxygens from (poly)ester or alkyl carbonates (−(C═O)O−R or RO−(C═O)−OR), based on the reported compounds in the NIST XPS database[15] and an XPS study on a polycarbonate-based (−O−R−O(C═O)O−R−) polymer electrolyte by Sun et al.[24]

F 1s Spectra. The F 1s environments (Figure 5a−d) of the surface layers formed on graphite electrodes show a strong dependence on the cell chemistry that is used. In the case of the Li cells, the formation of LiF (685.0 eV), for example, is commonly observed as a product of the electrolyte salt decomposition reaction of the PF_6^--anion.[25] The P−F environment of the anion itself is found as a separate component of the surface layer centered at around 687.1 eV.

https://doi.org/10.1021/acsaem.1c03491
ACS Appl. Energy Mater. XXXX, XXX, XXX−XXX

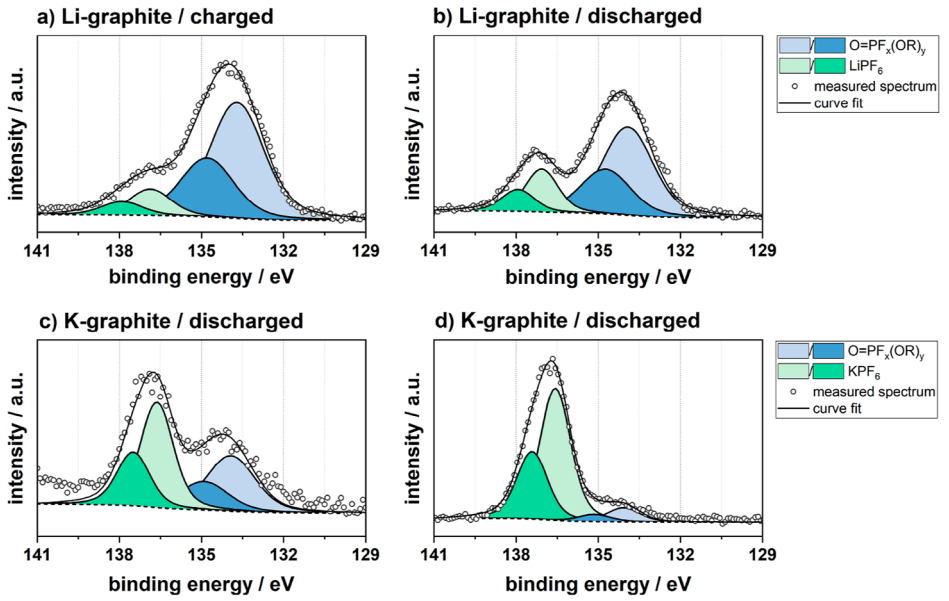

Figure 6. P 2p spectra of the graphite electrode surface after charge, that is, in the intercalation stage (a, c) and after the discharge, that is, in the deintercalated stage (b, d).

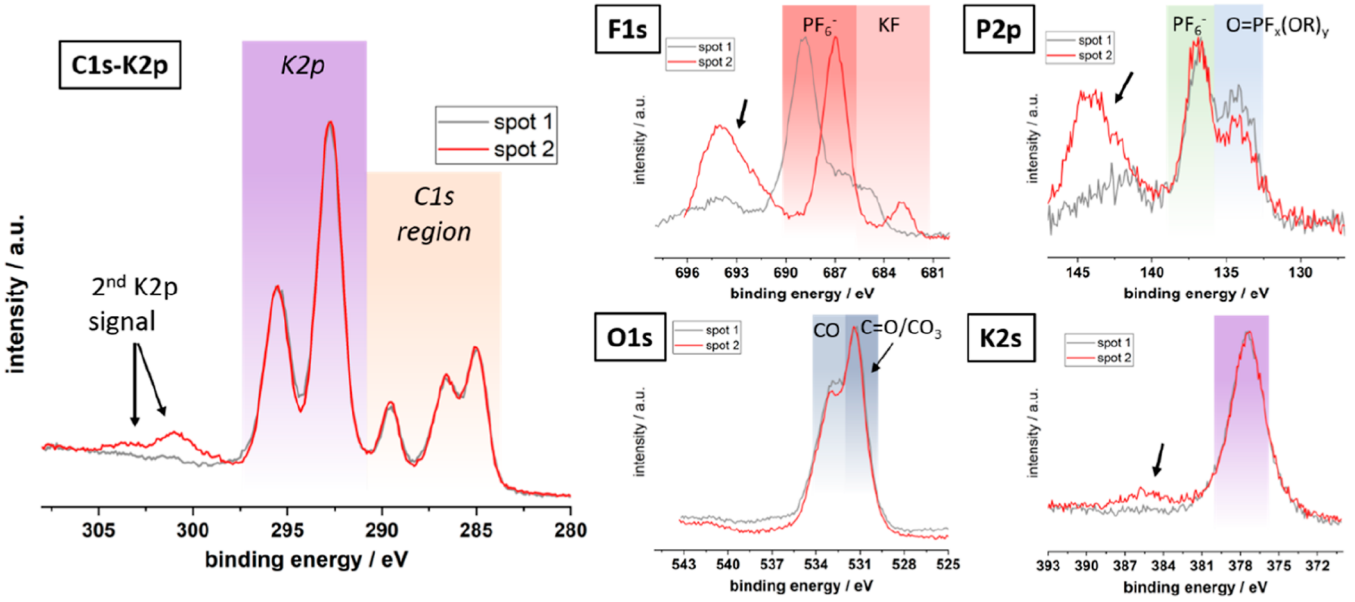

Figure 7. XPS spectra measured on two different spots on the same electrode sample, that is, a cycled graphite electrode vs K-metal stopped in the charged state after 1.5 cycles. The black arrows indicate regions where additional signals were observed.

In addition, a less-defined third component is observed that is generally ascribed to organic fluorides (e.g., the PVdF binder at around 688 eV[10]). However, as seen in Figure 5a,b the peak moves by nearly 2 eV between the charged to the discharged Li−graphite sample.

The F 1s spectra of the K−graphite samples are dominated by the KPF_6-species at 687.0 eV (charged)/686.9 eV (discharged). This comparison shows that the signal of the P−F bond remains largely unaffected by the choice of the anion. As already demonstrated in the reference measurements above, this is not the case for the fluorides, LiF and KF. In fact, in Figure 5c,d, a small signal is observed at around 682.8 eV that is assigned to KF, which is about 2.2 eV lower than that for LiF and also 0.6 eV lower than the BE measured for the reference sample. The broad feature above 690 eV in the F 1s spectrum of the charged K−graphite sample is a measurement artifact and will be discussed in more detail below.

P 2p Spectra. Similar to the F 1s spectra, the P 2p spectra show significant differences between electrodes cycled against lithium (Figure 6a,b) and those cycled against potassium (Figure 6c,d). The doublets marked in green are assigned to the P−F environment of the electrolyte salt at around 136.9 eV (P $2p_{3/2}$, Li−graphite) and 136.6 eV (P $2p_{3/2}$, K−graphite), respectively. As in the P−F environment of the F 1s spectra, the K-compounds are shifted to slightly lower BE. The blue peaks in the BE range between 133.8 and 134.1 eV (P $2p_{3/2}$) are ascribed to electrolyte degradation products, namely mono- and difluoroalkyl phosphates ($O{=}PF_x(OR)_y$).[22] A notable difference between the spectra of Li−graphite and K−graphite samples is the relative intensity ratios between the PF_6^- and

https://doi.org/10.1021/acsaem.1c03491
ACS Appl. Energy Mater. XXXX, XXX, XXX−XXX

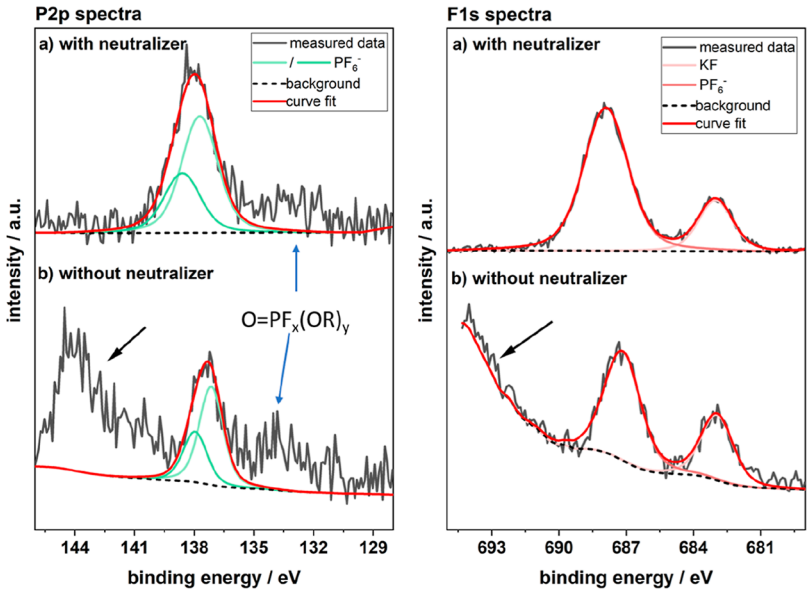

Figure 8. P 2p and F 1s spectra of a cycled graphite electrode (vs K, charged state) measured (a) with a neutralizer and (b) without a neutralizer to reveal charging effects. Charging artifacts are indicated with a black arrow.

phosphate signals: in the spectra of the Li−graphite samples, the PF_6^--signal is the smaller signal of the two, while in the spectra of the K−graphite samples, the intensity ratio is opposite, with the PF_6^--signal being the stronger one. It is important to highlight that at this point of the discussion relative intensities are discussed, since absolute signal intensities between different samples cannot be compared straightforwardly. The elemental distribution in the surface layer will be further discussed in the section below. As in the F 1s spectrum of the charged K−graphite sample, an additional signal above 140 eV is observed, which will be discussed in the following.

Charging Effects in the K 2s/K 2p, P 2p, and F 1s Spectra. The interpretation of the P 2p and F 1s spectra turned out to be challenging for K−graphite samples in the charged state, as artifacts appear in both BE regions. As shown in Figure 7 additional peaks appear in BE regions beyond the expected range in the C 1s−K 2p, F 1s, P 2p, and K 2s spectra (O 1s is not affected) that are indicated by black arrows. The feature appearing at 301.0 eV in the C 1s−K 2p spectrum comprises of two peaks separated by 2.7 eV, which is in good approximation with the BE difference between the K $2p_{3/2}$ and K $2p_{1/2}$ components. Thus, this feature could be assigned to an additional potassium species, although there are no reported compounds in the NIST XPS database beyond 298 eV.[15] This shift by about 7 eV is observed consistently between the peak maximum of the last "expected" signal and the signal artifact. Comparison with the XPS spectra acquired on a second spot on the sample further shows that not all parts of the sample surface are affected equally. Inhomogenously distributed, preferential charging effects were identified as the root cause of these signals in a separate experimental series, in which the measurements were repeated with and without charge neutralization during data acquisition (Figure 8), demonstrating that the artifacts disappear completely when the measurement is performed with a neutralizer. For reasons further explained below, the previous Figures 3−6 showed the data without the use of a neutralizer. The fact that the C 1s and O 1s environments were not affected by these charging effects strongly suggests that the signals are caused by electrolyte salt (KPF_6) residues. It is important to highlight that similar effects are not observed on electrode surfaces from graphite−Li half cells that have been prepared in the same way. In fact, KPF_6 exhibits a lower solubility in the carbonate solvent mixture than $LiPF_6$, which is why electrolyte salt concentrations of around 750−800 mM are commonly used in the literature, corresponding to concentrations just below the saturation limit. Therefore, it is likely that the rinsing step with DMC is not as efficient in removing KPF_6 salt residues as it is to remove $LiPF_6$. Additional experiments with other rinsing solutions (not shown), for example, based on an EC/DEC (v/v = 1:1) mixture, did show improvements in this regard. However, due to the higher solubility of salts in the presence of EC, the acquired XPS spectra showed notable changes in the SEI layer composition.

It should be noted that using charger neutralization also influenced the relative peak intensities and led to the less-defined C 1s and O 1s spectra (Figures S14 and S15). As these peaks are unrelated to KPF_6 deposits, this shows that charge neutralization may hinder SEI evaluation. Therefore, its use should always depend on the scientific question. If the aim is to get the overall salt accumulation on the electrode surface, a charge neutralization should be used to avoid the preferential charging of surface deposits. As the aim of our study is to evaluate the SEI in the K−graphite system and to compare its composition to the Li−graphite system, we chose to use measurements without a neutralizer to maintain the C 1s and O 1s structure. As the shift induced by the preferential charging in the K, F, and P spectra is quite large, this also allows excluding at least some of the surface deposits from the evaluation of the SEI composition. With this approach, some discrepancies remain in peak intensities and the BE position in the F 1s and P 2p spectra. For example, in the spectra acquired with a neutralizer, the peak positions agree better with the BEs reported in Table 1: the PF_6^- component in the F 1s spectra without neutralizer is observed at 687.1 eV, whereas with neutralization, the peak moved to a slightly higher BE of 687.9 eV, which agrees with the F 1s BE position reported for KPF_6

https://doi.org/10.1021/acsaem.1c03491
ACS Appl. Energy Mater. XXXX, XXX, XXX−XXX

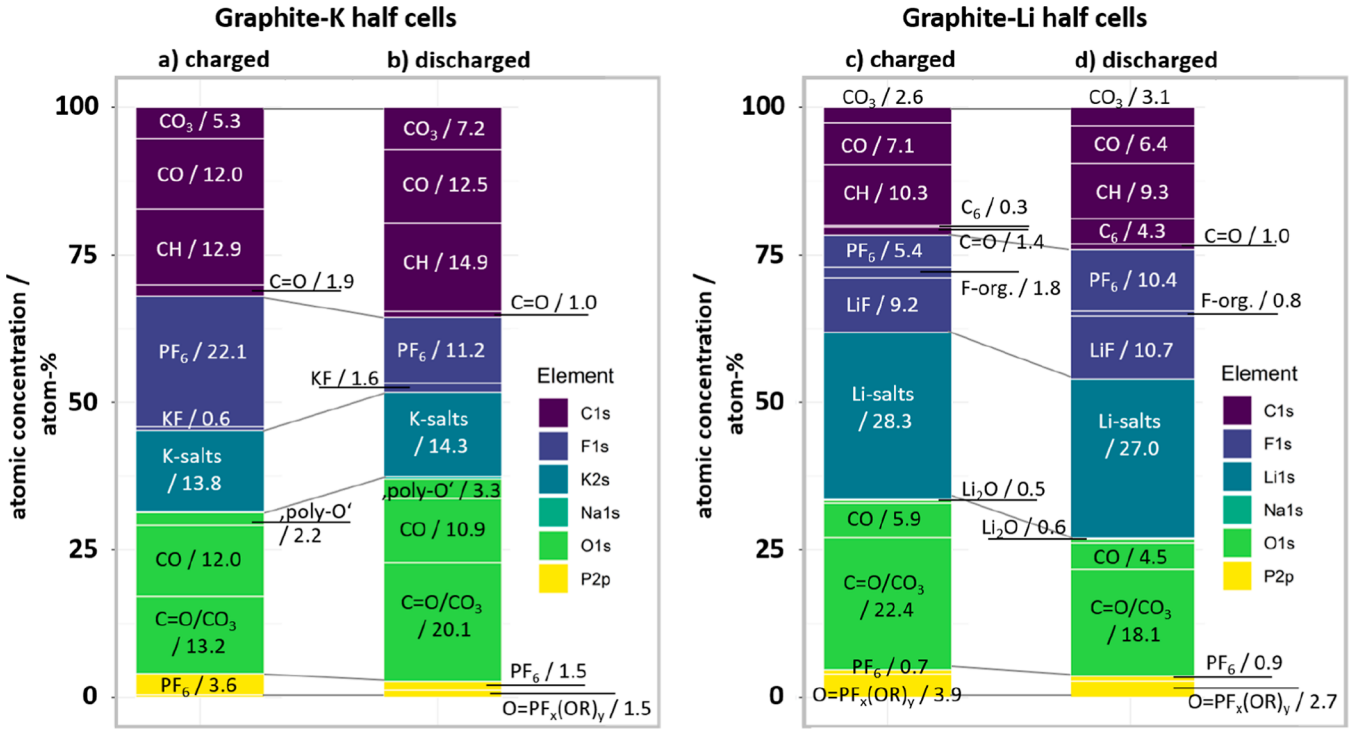

Figure 9. Bar plots of the atomic concentrations found of individual SEI components by XPS on (a) charged K−graphite, (b) discharged K−graphite, (c) charged Li−graphite, and (d) discharged Li−graphite electrodes.

in Table 1. The corresponding P 2p component is shifted accordingly. However, as indicated above, the degree of preferential charging differs in different spots on the sample and the fraction that experiences a shift is likely not an integral part of the SEI layer (see further discussion below). In other words, while the spectra recorded with charge neutralization might look better at first glance, they contain at least two fractions of salts, one of which is an artifact of the sample preparation.

DISCUSSION

In a previous study, we demonstrated that the cycle life of graphite electrodes cycled in potassium half cells is greatly reduced in comparison to the same electrode in a lithium half cell.[3] In this work, we now explore, if there are differences in the surface layer composition on graphite surfaces in the presence of either lithium or potassium ions and if these changes can be linked to the poor performance of graphite−K half cells. Except for the alkali metal, the systems were identical, using the same electrode composition and electrolyte components in both systems.

First significant differences were observed already during storage of the graphite electrodes against the respective alkali metal CE (OCV samples). In graphite−K half cells, potassium salts deposit rapidly over a couple of days. This so-called "crosstalk" event is nearly absent in the graphite−Li system. A control experiment with only the coin cell spacer as CE (CE-free samples) demonstrated that it is indeed the reactive K-metal CE that influences the surface composition of the graphite electrode early on. The results further highlight the higher reactivity of potassium versus electrolyte components, as compared to lithium. Similar trends during storage of a WE against potassium were recently reported by Madec et al. for an antimony composite electrode.[11]

Cycled electrodes were studied in charged (intercalated) and discharged (deintercalated) states. In the charged state, the spectra of the K−graphite samples showed artifacts at high binding energies in the K 2p, F 1s, P 2p, and K 2s regions, while the C 1s and O 1s regions remained unaffected. The signals were assigned to KPF_6 residues on the sample surface, presumably due to poor solubility of the potassium salt in DMC. In the F 1s spectrum, for example, these signals might be misinterpreted as those of organic fluorine-containing compounds. Furthermore, these artifacts might be overlooked when the BE region is chosen too narrow during data acquisition. The data suggest that there is a fraction of the KPF_6 salt that is in sufficient electronic contact, while other parts are not and hence experience a peak shift of about 7 eV to higher binding energies. This in turn means that the peak areas, particularly for the F 1s and P 2p components, cannot be accurately determined because it is unclear how much of the salt residue is affected by this charging effect. Conversely, when charge neutralization is used during data acquisition, the peaks merge into a single signal again, but in this case the fraction of the electrolyte salt residue remaining on the surface after washing is also unknown. Technically, this salt residue is not part of the SEI layer and should thus not be considered when determining the SEI's elemental composition (see below). This also raises the question regarding the interpretation of the F 1s and P 2p results of the cycled K−graphite sample (Figures 5 and 6). While the PF_6^- decomposition products LiF/KF and $O{=}PF_x(OR)_y$ are the dominant components in the F 1s and P 2p spectra of the Li−graphite samples (both charged and discharged), the trend is opposite for the corresponding spectra of the K−graphite samples. There, the KF appears only as a minor component due to the dominant PF_6^- signal (the fraction not affected by charging effects). The same applies to the P 2p spectra, although less pronounced.

https://doi.org/10.1021/acsaem.1c03491
ACS Appl. Energy Mater. XXXX, XXX, XXX−XXX

The KF signal is very weak in comparison to the PF_6^- signal. Low KF amounts presumably linked to solubility differences between LiF and KF in EC/DEC. To the best of our knowledge, KF solubilities in carbonate solvents have so far not been reported. However, previous comparisons between LiF and NaF suggest that the solubility in cyclic carbonates (pure or in mixtures with linear carbonates) is an order of magnitude higher for Na-salts.[13] Conversely, KPF_6 shows lower solubility in EC/DEC than the corresponding $LiPF_6$. Based on TGA measurements by Eshetu et al.,[26] it appears that $NaPF_6$ is thermally more stable than $LiPF_6$. While this is not enough to draw a trend, it is possible that softer cations improve the thermal stability. Thermal decomposition of $LiPF_6$ was identified as one reaction pathway to autocatalytic electrolyte decomposition and associated LiF formation.[25]

Another important observation is the differences in the SEI layer thickness between interphases formed in Li and K half cells. In the case of the Li−graphite samples, the graphite peak was visible in both the charged and discharged states. In the charged state, the SEI layer was just thin enough to still detect the graphite signal. In the discharged state, the SEI layer is generally thinner and therefore the graphite signal was clearly visible. In contrast, K−graphite electrodes neither showed the graphite signal in the charged nor in the discharged state, indicating that the surface layer is already considerably thicker after only 1.5 and 2 cycles, respectively. This result is correlated with previous findings, demonstrating that the voltage hysteresis is rapidly increasing in this setup.[3] A rapidly growing surface layer adds to the internal resistance of the cell and may cause a premature stop of the cycling sequence when the cutoff limit is reached but may also impede the electrochemical reaction and ion diffusion into the porous electrode.

For a more concise overview of the general differences between SEI layers formed on Li− and K−graphite (Figures 3−6), the atomic concentration (atom %; derived from the ratio between the normalized peak area and the sum of all normalized peak areas, as well as the instrument-specific sensitivity factors) of the individual SEI components are presented in Figure 9. A detailed list of the peak data from the above figures (Figures 3−6) and Figure 9 is provided in Tables S1−S4.

When comparing the atomic concentrations between the charged and discharged K−graphite samples, it can be noted that the overall C 1s and O 1s atomic fractions are larger in the SEI layer of the charged sample. This is primarily due to the fact that the carbonate content increased by about 2 atomic % in the carbon fraction, which translates to a 6 atomic % increase of the corresponding oxygen fraction (C═O/CO_3). In addition, an increase of the CH fraction by 2% is observed, suggesting the decomposition of the carbonate solvent. As mentioned above, the decomposition processes at the K-metal CE may influence the atomic concentrations in this regard. It is further observed that the PF_6 content decreased from the charged to the discharged sample considerably, that is, in the discharged sample, the PF_6 content is about half of that seen in the charged state, both for P 2p and F 1s signals. As stated above, the charged samples suffered from electrolyte salt residues that may affect the signal intensity, even though the charging artifact in the spectrum was not further considered in the curve fit and for the calculation of atomic concentrations. The reference measurements in Table 1 also suggest that the fluorine content is slightly overestimated with respect to the phosphorous content, assuming a 1:6 P/F ratio.

Furthermore, valuable information is gained from comparing the K−graphite SEI compositions to the corresponding Li−graphite samples. A brief look at the general elemental distribution shows that the Li-SEI comprises of a smaller carbon fraction and hence a less organic material. Especially, the LiF content is noteworthy, contributing to around 10 atomic % in both charged and discharged state to the overall SEI composition. For comparison, KF was nearly absent in the SEI of K−graphite samples, which might be partly attributed to different solubilities of the alkali metal fluorides of lithium and potassium. This trend is also reflected in an overall larger fraction of Li-salts that is twice as large as the K-salt fraction and includes both inorganic and organic salt deposits on the electrode surface. The increase of the carbon content in the discharged sample is mostly due to the presence of the graphite signal, which is technically not part of the SEI. Contrary to the SEI formed on K−graphite electrodes, the oxygen content is decreasing in the discharged state. Somewhat unexpected is the increase of the PF_6^- fraction in the F 1s signal from the charged sample (5.4 atomic %) to the discharged sample (10.4 atomic %), especially because the corresponding PF_6^- signal in the P 2p spectrum did not change to the same extent. From the atomic concentrations of the P 2p fractions, it appears as if the PF_6^- fraction in the F 1s spectrum of the charged sample is underestimated. This is likely due to the preferential charging effects discussed above.

CONCLUSIONS

A detailed XPS analysis was performed on graphite electrodes cycled either in a lithium or potassium half cell. In order to aid the assignment of potassium species in the SEI formed of K−graphite samples, reference measurements were conducted on selected characteristic SEI compounds (e.g., KF, KPF_6) or closely related compounds (e.g., CH_3COOK). Measurements on the electrode surfaces after storage under OCV conditions showed that the surface layer is influenced early on due to deposition of electrolyte decomposition products that have formed at the reactive potassium CE of the half cell. Despite the system parameters (electrode and electrolyte composition) being the same, with exception of the cation of the electrolyte salt and the alkali metal as CE, the SEI layers of the graphite electrodes differed considerably after only two cycles. In the light of the earlier results on the significantly reduced cycling stability of K−graphite electrodes, as well as the poor first-cycle CEs, we herein conclude that the SEI thickness and its more organic character represent a hindrance to the extended cycle life. This might be because organic compounds generally show a higher tendency to dissolve in the electrolyte as compared to inorganic salts, such as KF. In the SEI layer of the Li−graphite cell, the LiF fraction not only remained stable but also contributed with a significant content of around 10 atom %. In contrast, the KF content in K−graphite systems is less than 2 atom %, while the PF_6^- content varies strongly between the charged and discharged samples. The origins of this behavior are not entirely clear but are likely related to different solubilities of the alkali metal fluorides and the thermal/chemical stability of the PF_6-anion. Higher solubilities lead to recurrent SEI reformation reactions culminating in rapid SEI layer growth, as has been seen in this study. Fast SEI layer growth may also be associated with the rapid buildup of voltage hysteresis in cycling experiments, although this process

https://doi.org/10.1021/acsaem.1c03491
ACS Appl. Energy Mater. XXXX, XXX, XXX−XXX

is not only associated with the graphite electrode but also the reactive potassium metal CE. Our results highlight that implementing reliable and long-lasting graphite electrodes for KIB applications will require more work on the design of more-stable interphases. One avenue for the future could be targeting higher fractions of inorganic, insoluble compounds in the SEI, for instance as in previous attempts to enrich electrolytes with cosalts.[13,27]

■ ASSOCIATED CONTENT

Supporting Information

The Supporting Information is available free of charge at https://pubs.acs.org/doi/10.1021/acsaem.1c03491.

Additional XPS spectra of the reference samples; spectra of the OCV and CE-free samples; and charging effects and voltage profiles of cycled Li− and K−graphite half cells (PDF)

■ AUTHOR INFORMATION

Corresponding Author

Fabian Jeschull − *Institute for Applied Materials-Energy Storage Systems (IAM-ESS), Karlsruhe Institute of Technology (KIT), 76344 Eggenstein-Leopoldshafen, Germany*; orcid.org/0000-0002-5927-1978; Email: fabian.jeschull@kit.edu

Authors

Franziska Allgayer − *Institute for Applied Materials-Energy Storage Systems (IAM-ESS), Karlsruhe Institute of Technology (KIT), 76344 Eggenstein-Leopoldshafen, Germany*

Julia Maibach − *Institute for Applied Materials-Energy Storage Systems (IAM-ESS), Karlsruhe Institute of Technology (KIT), 76344 Eggenstein-Leopoldshafen, Germany*; orcid.org/0000-0003-1339-7804

Complete contact information is available at: https://pubs.acs.org/10.1021/acsaem.1c03491

Notes

The authors declare no competing financial interest.

■ ACKNOWLEDGMENTS

This work contributes to the research performed within the Post Lithium Storage Cluster of Excellence (POLiS), funded by the Deutsche Forschungsgemeinschaft (DFG, German Research Foundation) under Germany's Excellence Strategy—EXC 2154—Project number 390874152, as well as to the research performed at the Center for Electrochemical Energy Storage Ulm-Karlsruhe (CELEST). Furthermore, F.J. gratefully acknowledges the German Research Foundation for financial support (grant #448719339) within the framework of the bilateral German−Russian research projects (RFBR-DFG Cooperation).

■ REFERENCES

(1) Zhao, J.; Zou, X.; Zhu, Y.; Xu, Y.; Wang, C. Electrochemical Intercalation of Potassium into Graphite. *Adv. Funct. Mater.* **2016**, *26*, 8103−8110.

(2) Komaba, S.; Hasegawa, T.; Dahbi, M.; Kubota, K. Potassium Intercalation into Graphite to Realize High-Voltage/High-Power Potassium-Ion Batteries and Potassium-Ion Capacitors. *Electrochem. Commun.* **2015**, *60*, 172−175.

(3) Jeschull, F.; Maibach, J. Inactive Materials Matter: How Binder Amounts Affect the Cycle Life of Graphite Electrodes in Potassium-Ion Batteries. *Electrochem. Commun.* **2020**, *121*, 106874.

(4) Carboni, M.; Naylor, A. J.; Valvo, M.; Younesi, R. Unlocking High Capacities of Graphite Anodes for Potassium-Ion Batteries. *RSC Adv.* **2019**, *9*, 21070−21074.

(5) Jian, Z.; Luo, W.; Ji, X. Carbon Electrodes for K-Ion Batteries. *J. Am. Chem. Soc.* **2015**, *137*, 11566−11569.

(6) Igarashi, D.; Kubota, K.; Hosaka, T.; Tatara, R.; Inose, T.; Ito, Y.; Inoue, H.; Takeuchi, M.; Komaba, S. Effect of Crystallinity of Synthetic Graphite on Electrochemical Potassium Intercalation into Graphite. *Electrochemistry* **2021**, *89*, 433−438.

(7) Verma, P.; Maire, P.; Novák, P. A Review of the Features and Analyses of the Solid Electrolyte Interphase in Li-Ion Batteries. *Electrochim. Acta* **2010**, *55*, 6332−6341.

(8) Malmgren, S.; Ciosek, K.; Hahlin, M.; Gustafsson, T.; Gorgoi, M.; Rensmo, H.; Edström, K. Comparing Anode and Cathode Electrode/Electrolyte Interface Composition and Morphology Using Soft and Hard X-Ray Photoelectron Spectroscopy. *Electrochim. Acta* **2013**, *97*, 23−32.

(9) Obrovac, M. N.; Chevrier, V. L. Alloy Negative Electrodes for Li-Ion Batteries. *Chem. Rev.* **2014**, *114*, 11444−11502.

(10) Naylor, A. J.; Carboni, M.; Valvo, M.; Younesi, R. Interfacial Reaction Mechanisms on Graphite Anodes for K-Ion Batteries. *ACS Appl. Mater. Interfaces* **2019**, *11*, 45636−45645.

(11) Madec, L.; Gabaudan, V.; Gachot, G.; Stievano, L.; Monconduit, L.; Martinez, H. Paving the Way for K-Ion Batteries: Role of Electrolyte Reactivity through the Example of Sb-Based Electrodes. *ACS Appl. Mater. Interfaces* **2018**, *10*, 34116−34122.

(12) Mogensen, R.; Brandell, D.; Younesi, R. Solubility of the Solid Electrolyte Interphase (SEI) in Sodium Ion Batteries. *ACS Energy Lett.* **2016**, *1*, 1173−1178.

(13) Ma, L. A.; Naylor, A. J.; Nyholm, L.; Younesi, R. Strategies for Mitigating Dissolution of Solid Electrolyte Interphases in Sodium-Ion Batteries. *Angew. Chem.* **2021**, *133*, 4905−4913.

(14) Pfeifer, K.; Arnold, S.; Becherer, J.; Das, C.; Maibach, J.; Ehrenberg, H.; Dsoke, S. Can Metallic Sodium Electrodes Affect the Electrochemistry of Sodium-Ion Batteries? Reactivity Issues and Perspectives. *ChemSusChem* **2019**, *12*, 3312−3319.

(15) Naumkin, A. V.; Kraut-Vass, A.; Gaarenstroom, S. W.; Powell, C. J. *NIST X-ray Photoelectron Spectroscopy Database*.

(16) Caracciolo, L.; Madec, L.; Martinez, H. XPS Analysis of K-Based Reference Compounds to Allow Reliable Studies of Solid Electrolyte Interphase in K-Ion Batteries. *ACS Appl. Energy Mater.* **2021**, *4*, 11693.

(17) Shchukarev, A.; Korolkov, D. XPS Study of Group IA Carbonates. *Cent. Eur. J. Chem.* **2004**, *2*, 347−362.

(18) Kubota, K.; Dahbi, M.; Hosaka, T.; Kumakura, S.; Komaba, S. Towards K-Ion and Na-Ion Batteries as "Beyond Li-Ion". *Chem. Rec.* **2018**, *18*, 459−479.

(19) Ciosek Högström, K.; Malmgren, S.; Hahlin, M.; Gorgoi, M.; Nyholm, L.; Rensmo, H.; Edström, K. The Buried Carbon/Solid Electrolyte Interphase in Li-Ion Batteries Studied by Hard x-Ray Photoelectron Spectroscopy. *Electrochim. Acta* **2014**, *138*, 430−436.

(20) Leroy, S.; Blanchard, F.; Dedryvère, R.; Martinez, H.; Carré, B.; Lemordant, D.; Gonbeau, D. Surface Film Formation on a Graphite Electrode in Li-Ion Batteries: AFM and XPS Study. *Surf. Interface Anal.* **2005**, *37*, 773−781.

(21) Philippe, B.; Hahlin, M.; Edström, K.; Gustafsson, T.; Siegbahn, H.; Rensmo, H. Photoelectron Spectroscopy for Lithium Battery Interface Studies. *J. Electrochem. Soc.* **2016**, *163*, A178−A191.

(22) Jeschull, F.; Maibach, J.; Félix, R.; Wohlfahrt-Mehrens, M.; Edström, K.; Memm, M.; Brandell, D. Solid Electrolyte Interphase (SEI) of Water-Processed Graphite Electrodes Examined in a 65 mAh Full Cell Configuration. *ACS Appl. Energy Mater.* **2018**, *1*, 5176−5188.

(23) Onuma, H.; Kubota, K.; Muratsubaki, S.; Hosaka, T.; Tatara, R.; Yamamoto, T.; Matsumoto, K.; Nohira, T.; Hagiwara, R.; Oji, H.; Yasuno, S.; Komaba, S. Application of Ionic Liquid as K-Ion

Electrolyte of Graphite//K2Mn[Fe(CN)6] Cell. *ACS Energy Lett.* **2020**, *5*, 2849−2857.
(24) Sun, B.; Xu, C.; Mindemark, J.; Gustafsson, T.; Edström, K.; Brandell, D. At the Polymer Electrolyte Interfaces: The Role of the Polymer Host in Interphase Layer Formation in Li-Batteries. *J. Mater. Chem. A* **2015**, *3*, 13994−14000.
(25) Campion, C. L.; Li, W.; Lucht, B. L. Thermal Decomposition of LiPF[sub 6]-Based Electrolytes for Lithium-Ion Batteries. *J. Electrochem. Soc.* **2005**, *152*, A2327−A2334.
(26) Eshetu, G. G.; Grugeon, S.; Kim, H.; Jeong, S.; Wu, L.; Gachot, G.; Laruelle, S.; Armand, M.; Passerini, S. Comprehensive Insights into the Reactivity of Electrolytes Based on Sodium Ions. *ChemSusChem* **2016**, *9*, 462−471.
(27) Komaba, S.; Itabashi, T.; Kimura, T.; Groult, H.; Kumagai, N. Opposite Influences of K+ versus Na+ Ions as Electrolyte Additives on Graphite Electrode Performance. *J. Power Sources* **2005**, *146*, 166−170.

https://doi.org/10.1021/acsaem.1c03491
ACS Appl. Energy Mater. XXXX, XXX, XXX−XXX